Wind and Structures, Vol. 13, No. 5 (2010) 385-412
DOI: http://dx.doi.org/10.12989/was.2010.13.5.385

Physical modelling of a downdraft outflow with a slot jet

W.E. Lin*[a] and E. Savory[b]

Department of Mechanical and Materials Engineering, The University of Western Ontario, London, Ontario, Canada, N6A 5B9

(Received September 15, 2009, Accepted March 3, 2010)

Abstract. This article provides a time-resolved characterisation of the wind field in a recently-commissioned, downdraft outflow simulator at The University of Western Ontario. A large slot jet approach to physical simulation was used. The simulator performance was assessed against field observations from a 2002 downdraft outflow near Lubbock, Texas. Outflow wind speed records were decomposed according to classical time series analysis. Length scales, characterising the coarse and fine flow structure, were determined from the time-varying mean and residual components, respectively. The simulated downdraft outflow was approximately 1200 times smaller in spatial extent than the 2002 Lubbock event.

Keywords: downdraft outflow; downburst; microburst; localised high-intensity wind; wind tunnel; slot jet; mixing layer; transient signal; time series analysis.

1. Introduction

The boundary layer wind tunnel has had a remarkable progression from the nascent work in the 1950s to its current role as a refined structural design tool. It is used to simulate near-surface synoptic winds, where wind speed can be approximated as statistically stationary. It is well-known that statistically non-stationary, surface-level outflows from storms have different characteristics than boundary layer winds. Observations by the meteorological community (reviewed by Wakimoto 2001) indicate extreme thunderstorm winds are associated with downdraft outflows. Since these extreme wind speeds may represent the design loads in many locales, physical test facilities have been developed to simulate a downdraft outflow. The engineering challenge is to achieve a sufficiently large flow such that the effect of a simulated downdraft outflow on properly-scaled structural models can be studied. The present approach (a slot jet installed in a pre-existing large boundary layer wind tunnel) was motivated by this challenge.

Letchford *et al.* (2002) reviewed the early work on physical simulation of downdraft outflows. The conventional approach to downdraft simulation utilised a jet impinging on a flat surface (Walker 1992). The most sophisticated simulations with this approach used a moving jet nozzle (Letchford and Chay 2002, Sengupta and Sarkar 2008) or an actuated aperture at the nozzle (Mason *et al.* 2005, McConville *et al.* 2009). Recent development of impinging jet facilities is towards larger

* Corresponding Author, Graduate Student, E-mail: wlin26@uwo.ca
[a]Graduate Student
[b]Associate Professor

jet nozzles (e.g., 1 m diameter used by McConville *et al*. 2009) to promote fully-turbulent flow.

The objective of the present alternative approach (Lin and Savory 2006, Lin *et al*. 2007) was to simulate only the high-intensity convective downdraft winds near the planetary surface, as this is where most built structures are found. By limiting the simulation domain, a significantly larger scale was achievable, whilst retaining the main features of a convective downdraft outflow. Following the approach of Choi and Hidayat (2002) and Holmes *et al*. (2008), statistically non-stationary wind speed records were separated into mean and residual components by a moving-average procedure. Hereafter, Holmes *et al.* (2008) is abbreviated as H2008.

The facility design and implementation of the downdraft outflow simulator in Wind Tunnel 1 (WT1 DOS) at The University of Western Ontario (UWO) are described in § 2. The hot-wire anemometry set-up and the time-resolved point measurements of wind speed are presented. Analysis of the wind speed in a 2002 rear-flank downdraft outflow (2002 RFD), observed by Orwig and Schroeder (2007), is included to allow a comparison with the simulator results. § 3 compares the time-varying mean components from the WT1 DOS and the 2002 RFD data. § 4 compares the residual component (i.e., the fluctuations about the time-varying mean). Although the former component is of primary concern for designing structures to withstand the extreme loads in this type of wind event, the latter component may have implications for dynamic behaviour or oscillatory response of certain structures. § 5 presents the conclusions of this study and the direction of future work. A nomenclature section defines the symbols and abbreviations used in this article.

2. Description of the simulator

2.1 Facility development

The prototype (1:11 scale) of Lin *et al*. (2007) indicated that a slot jet facility can generate the following downdraft outflow features: (1) a dominant horizontal roll vortex, (2) the signature wind speed history, and (3) the expected vertical profile of ensemble-averaged wind speed. The following criteria guided the facility design process:

1. The test section flow must be sufficiently large to model wind effects on built structures. The simulator design was based on modification of existing infrastructure. This approach made optimal use of existing facilities and minimised the overall facility cost.
2. The simulator must generate the signature wind speed history observed from downdraft outflows. A gated nozzle enabled flow pulsation.
3. The ability to augment an outflow wind speed profile with varying levels of ambient winds is desirable. The pre-existing suck-down fan readily generated an ambient flow. This ambient flow and the slot jet formed a co-flow, which can be likened to a gust front encountering an ambient wind field that contributes to the gust front intensity.
4. The ability to successively test the same structural model under conventional atmospheric boundary layer and downdraft outflow conditions, within the same facility, is desirable.

Storm translation and outflow pulsation with an impinging jet approach have been modelled by other investigators by moving fan equipment on rails (Letchford and Chay 2002, Sengupta and Sarkar 2008) and using intricate nozzle apertures (Mason *et al.* 2005, McConville *et al*. 2009). A slot jet approach is less cumbersome in terms of the requisite equipment and test procedures. The trade-off is that the outflow features are modelled by a plane mixing layer rather than an impinging jet.

2.2 Facility characteristics

Wind Tunnel 1 at UWO is an open-return wind tunnel. In operation, negative gauge pressure is induced in the working section. Along the working section fetch (X = 30 m), the tunnel height increases linearly (from Y = 1.68 to 2.21 m) to minimise the adverse pressure gradient from test model and roughness element blockage. The tunnel span is Z = 2.44 m. A fan at the end of the fetch draws air through the working section and is capable of generating wind speeds of up to 15 m/s.

A secondary flow was added, at the working section floor, for downdraft outflow simulation. As shown by Fig. 1, the simulator assembly was located in the first 7.5 m of fetch. In regular boundary layer testing, the suck-down fan generated a flow from right to left in the figure. Twin centrifugal blowers generated the secondary flow (Views A & B, Fig. 1). The design flow rate was (2 × 4.7) m^3/s at a pressure rise of 2 kPa. The blowers expelled ambient air into a Y-shaped diffuser that (1) expanded the cross-sectional flow area of the blower outlets to that of the duct, and (2) merged the two streams into a single stream. The duct led to vanes that turned the flow through 180º (View C). This section also contracted the flow cross-section height by a 6:1 ratio, leading to a slot nozzle height of b = 159 ± 2 mm across the 2.44 m span. Slot top thickness was minimised to 4.8 mm with the aid of two support ribs at the side walls and two more ribs at the span-wise 1/3 positions. Each

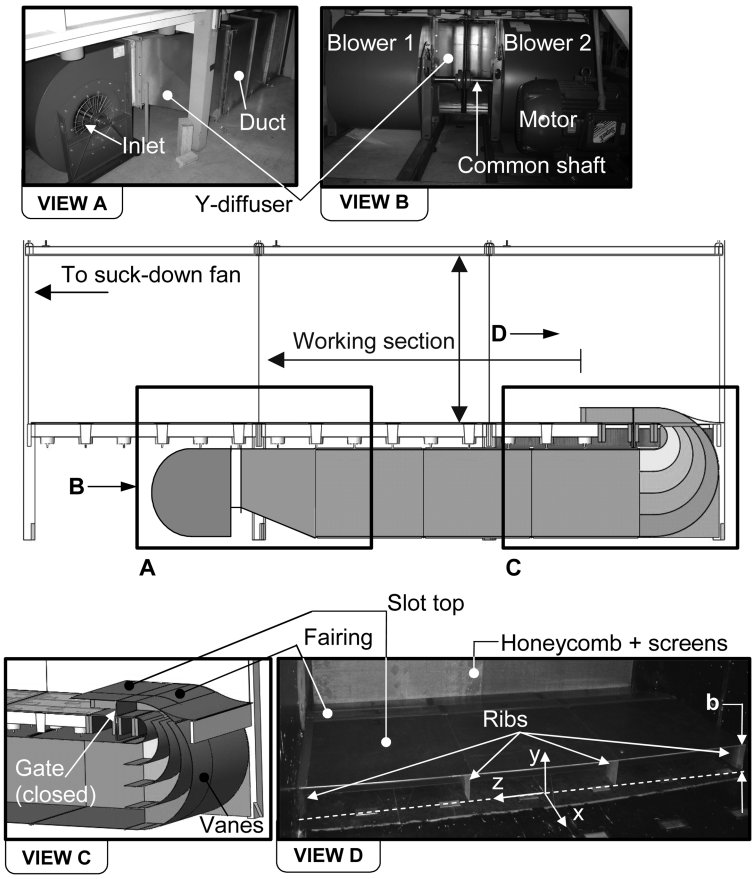

Fig. 1 Overview of the WT1 DOS assembly and nomenclature

rib had a span-wise thickness of 10.3 mm and tapered to a sharp edge at its downstream end. A Cartesian co-ordinate system was used for this article (View D). The upstream end of the slot top was faired to the working section floor using an S-shaped profile that covered the first 0.62 m (3.8 b) of fetch. The slot top extended a further 0.79 m (4.9 b) downstream, terminating as the nozzle lip.

A metal plate (6.35 mm thickness) was used to pulse the slot jet (View C). This gate extended across the entire tunnel span. Its motion was limited to vertical translation. The fully-closed and fully-open gate positions were flush with the slot top and working section floor, respectively. The gate was driven by two linear actuators whose motion was synchronised through software. The actuators were rated with ± 0.025 mm repeatability and ± 0.400 mm accuracy. The gate was retractable below the floor, the slot apparatus was removable, and the facility was readily converted back to boundary layer testing within two person-hours of labour.

2.3 Anemometry and measurement procedures

Flow visualisations were performed to assess the development of the pulsed slot jet. The tracer particles were an aqueous aerosol of glycol and water droplets. A 4.1 mega-pixel digital camera captured video at a rate of 30 frames per second.

Wind speed histories were acquired using a Dantec Dynamics StreamLine constant temperature anemometry system. Single (55P11) and cross (55P61) hot-wire probes were used. Hereafter, the single and cross hot-wire probes are referred to as SHW and CHW, respectively. Signal conditioning was applied to maximise the voltage range. The signals were low-pass filtered at 30 kHz and data were acquired by a PC at a sampling rate of 60 kHz. The hot-wires were calibrated using a Dantec 90H01 unit. The expected accuracy of wind speed measurements was ± 5%.

Each outflow simulation began with the twin blowers in steady-state operation and the gate fully-closed. A static pressure was built up within the ducting between the blowers and the rear face of the gate. After attaining steady internal pressure in the ducting, the gate was lowered to its fully-open position and then immediately returned to its fully-closed position. This procedure released a single slot jet pulse into the working section.

Aside from the opposing direction of motion, the opening and closing phases of the gate were configured identically. The displacement history of the gate was trapezoidal in each direction, as it moved across the slot height. Peak gate speed and acceleration were 1 m/s and 10 m/s^2, respectively. The gate actuation duration was 0.3 s (i.e., from the instant the gate began opening to its return to top-dead position). The wind tunnel suck-down fan was also in steady operation. The ratio of the ambient wind speed to the slot jet wind speed was set as 1:3, because the 2002 RFD gust front speed was 12 m/s (H2008) with peak speed of 40 m/s.

2.4 Initial flow conditions

Wind speed measurements of the steady slot jet with no co-flow were performed to characterise the slot jet initial conditions. Vertical profiles were obtained across the 160 mm slot height at three different span-wise positions (Fig. 2). The slot span was divided into three compartments by the two ribs shown in Fig. 1 (View D), and the Fig. 2 profiles were at the three mid-compartment span-wise locations.

At the nozzle exit, the slot jet included boundary layers at the working section floor and the bottom face of the slot top. These two boundary layers flanked the jet core that had relatively

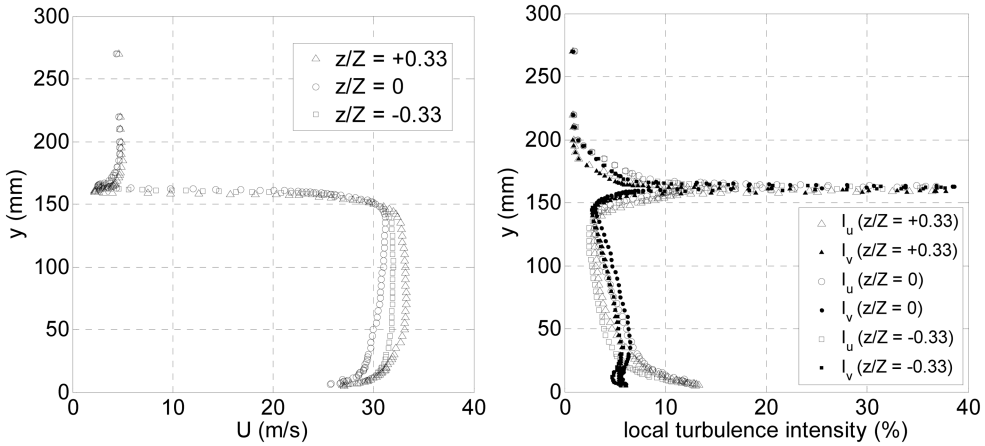

Fig. 2 Vertical profiles at x/b = 0.04 (WT1 DOS)

Table 1 Characteristics of the boundary layers at the slot nozzle (WT1 DOS, x/b = 0.04, CHW)

	Bottom surface of slot top			Floor surface		
z/Z	δ*/b	Θ/b	H	δ*/b	Θ/b	H
0.33	0.021	0.015	1.4	0.032	0.021	1.5
-0.33	0.012	0.010	1.2	0.024	0.016	1.5
0	0.006	0.006	1.1	0.042	0.030	1.4

uniform mean wind speed. The variation across the central 60% of the slot height was within ± 4% of the slot exit bulk wind speed. Across most of the slot height, both turbulence intensity components were in the range of 2 to 6%.

Displacement and momentum thicknesses were calculated to characterise the initial conditions at the slot nozzle. Simpson's rule was used for piecewise integration between the maximum wind speed point and the nearest measurement to a solid boundary. The contribution to the integral from the region between a solid boundary and its nearest measurement point was determined by applying a no-slip condition at the floor and performing a polynomial fit. With the polynomial function, an exact integral was evaluated.

The plate wake was negligibly thin compared to the slot height, as shown by Fig. 2 and the boundary layer thicknesses summarised in Table 1. The boundary layer at the floor was consistently thicker than that at the slot top, for the three span-wise positions. Shape factor ($H = \delta^*/\Theta$) is a good indicator of pressure gradient. The shape factor of turbulent flow over a flat plate is 1.3. With increasing adverse pressure gradient, separation occurs at H = 2.4 (White 2003, p. 473). The shape factors in Table 1 indicated that pressure gradient effects were minimal at the slot nozzle.

2.5 Downstream flow conditions

A flow pulse from the WT1 DOS was visualised and a video record showed the passage of the burst front (Fig. 3) at about ten slot heights downstream of the nozzle (x/b = 10). The dominant vortex, associated with peak wind speed, was identifiable. A sense of the outflow size was gained

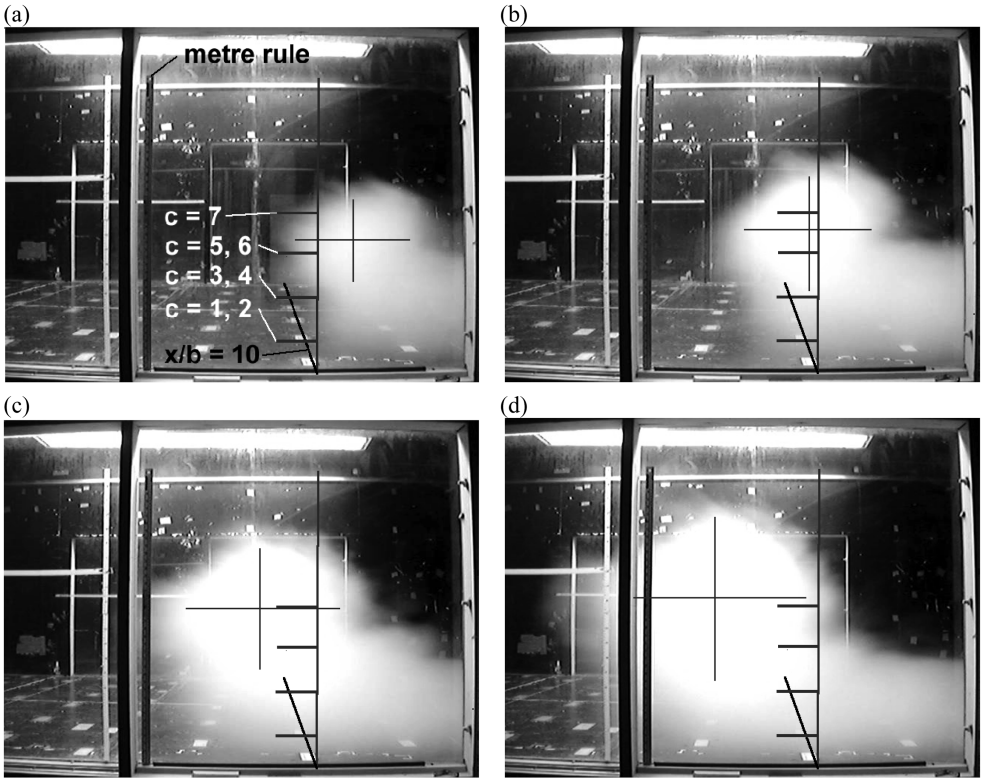

Fig. 3 Flow visualisation from the WT1 DOS (1/15 s between successive frames)

by comparison to the metre rule affixed to the working section window.

As described by Fujita (1981, Figs. 27 and 28), the dominant vortex concurrently moved away from the surface boundary and the downdraft column. Mason *et al.* (2005, Fig. 8) observed this type of behaviour for a pulsed impinging jet and described the trajectory of the core of the dominant vortex with a cubic polynomial function. For the WT1 DOS, a best-fit cubic polynomial function ($R^2 = 0.9902$) was found to be suitable as well. A trajectory plot has x- and y-position axes, and each plotted point occurs at a different time.

Velocity measurements were conducted with seven different SHW and CHW configurations (Table 2). In each configuration, the two probes were located at the same streamwise (x) and

Table 2 CHW probe locations (WT1 DOS)

c	y/b	z/Z
1	0.63	-0.41
2	0.63	+0.40
3	1.56	-0.41
4	1.56	+0.40
5	2.50	-0.41
6	2.50	+0.40
7	3.44	-0.41

vertical (y) position. However, the SHW was always positioned at mid-span (z = 0), and the CHW was always offset to one side (z < 0 or z > 0).

Fig. 4 shows a wind speed history as acquired from the SHW. The gate actuation and anemometry systems were synchronised within the limitations of the Labview control software, which had accuracy on the order of milliseconds. The downward motion of the gate and the data acquisition from the anemometer were initiated simultaneously at t = 0.

2.5.1 Ensemble-averaging

Multiple hot-wire measurements were conducted under identical conditions. The resulting collection of wind speed histories was an ensemble of sample functions or trials, which describes the non-stationary random process, {u(c, k, t)}. The ensemble-average, <U>, was estimated by performing instantaneous averages over the ensemble of trials forming the process, as described by Eq. (1). For instance, u(1, 1, t) in Fig. 4 was one of the nine trials that were averaged to determine <U(1, t)>, the ensemble-average in Fig. 5. The parameters, annotated on Fig. 5, are described in the Nomenclature.

$$\langle U \rangle = \frac{1}{K} \sum_{k=1}^{K} u(c, k, t) \tag{1}$$

2.5.2 Sample function averaging

A statistically non-stationary wind speed sample function can be separated into average and residual components. The decomposition involved calculating a central moving-average (i.e., a "running mean") from the acquired signal, and then calculating the residual as the instantaneous difference between the acquired signal and running mean. Amongst the various digital signal processing procedures available, a moving-average procedure was an appropriate choice for filtering the random fluctuations from a time domain, digital signal, whilst retaining a sharp step response in the average component. For example, the wind speed history in Fig. 4 was decomposed into the

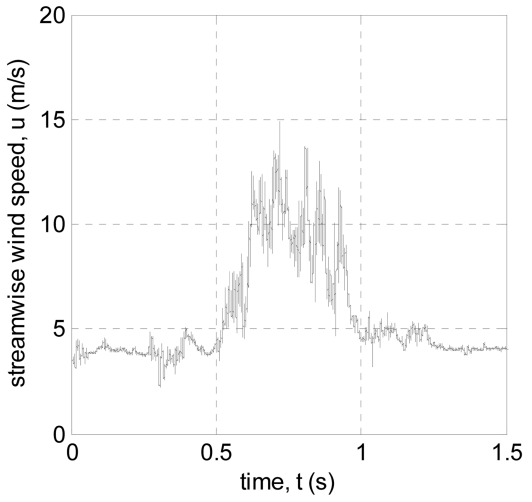

Fig. 4 Wind speed history from SHW probe (WT1 DOS, c=1, k=1)

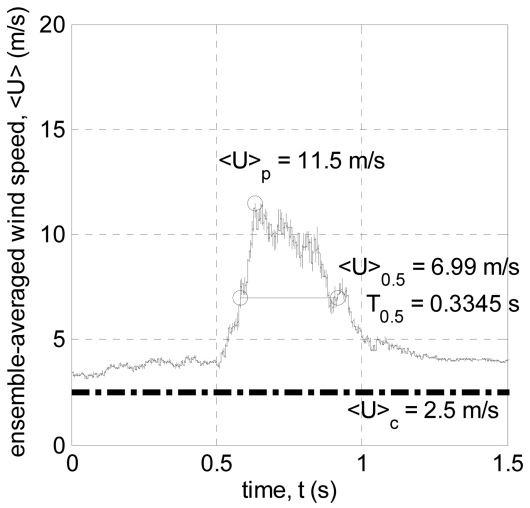

Fig. 5 Ensemble-averaged wind speed history from SHW probe (WT1 DOS, c = 1, K = 9)

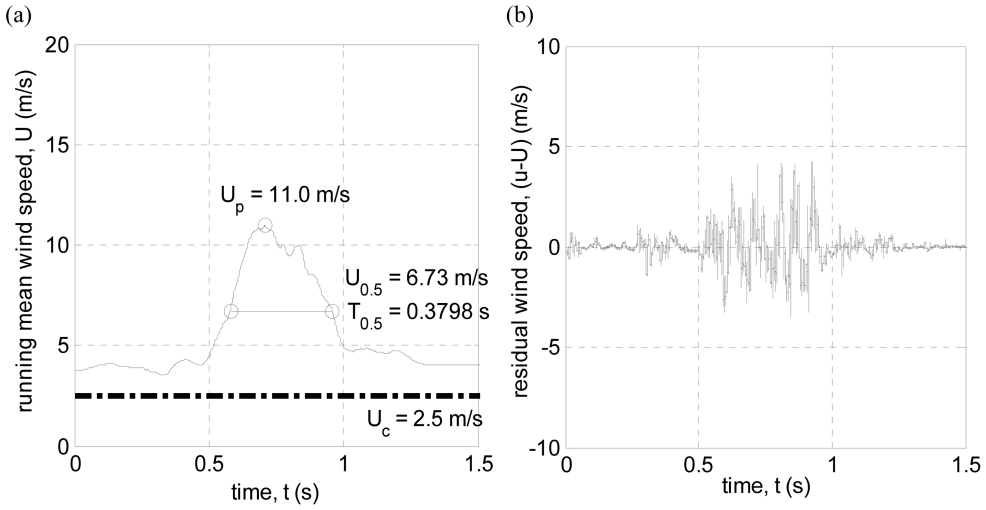

Fig. 6 (a) Running mean and (b) residual wind speed history (WT1 DOS, SHW probe, c = 1, k = 1)

running mean in Fig. 6(a) and the residual in Fig. 6(b).

H2008 suggested the following criteria for determining an appropriate averaging time (i.e., the "window" or "filter duration", T_W): (1) large-scale peaks and troughs in the acquired signal should be retained by the running mean, (2) the time-average of the residual signal should vanish, and (3) the local effect of the filter duration on gust factor should be minimal (i.e., $\partial G / \partial T_W \to 0$ at the selected T_W). Based on these criteria, a filter size of M = 5000 samples was selected. Figs. 7 and 8 show the findings for the simulated outflow measurements (compare to Figs. 6 and 10 of H2008). The selected filter duration for this study was $T_W = M/f_s$ = (5000 samples) / (60000 Hz) = 0.083 s. In dimensionless terms, $T_W/T_{0.5}$ = 25% for the SHW data and 31% for the CHW data. H2008 selected $T_W/T_{0.5}$ = 40 s/160 s = 25% for the 2002 RFD data.

With an appropriate value of M, the running mean wind speed was determined with a central moving-average calculation. For most of the u signal, there existed at least M/2 samples before and after the j-th point being calculated, permitting a full window to be used. Approaching the leading and trailing edges of the signal, the window incrementally reduces to one-sided about j, with a width of M/2 samples.

A random process is ergodic if its ensemble-average is equal to the corresponding sample function average from any single record (Bendat and Piersol 1986). Comparison of Figs. 5 and 6(a) gave an indication of the ergodicity of the non-stationary outflow wind speed process. Further detailed comparisons indicated that, near the instant of peak gust occurrence, the ensemble-average was representative of the running mean. The high-frequency fluctuations of the ensemble-average would be smoothed out by increasing the ensemble size - in which case, Eq. (2) would be a reasonable statement.

$$\lim_{K \to \infty} \langle U \rangle = U(c, t) \tag{2}$$

The ergodicity property is useful because it allays the necessity of performing numerous trials since a single trial is representative of the process.

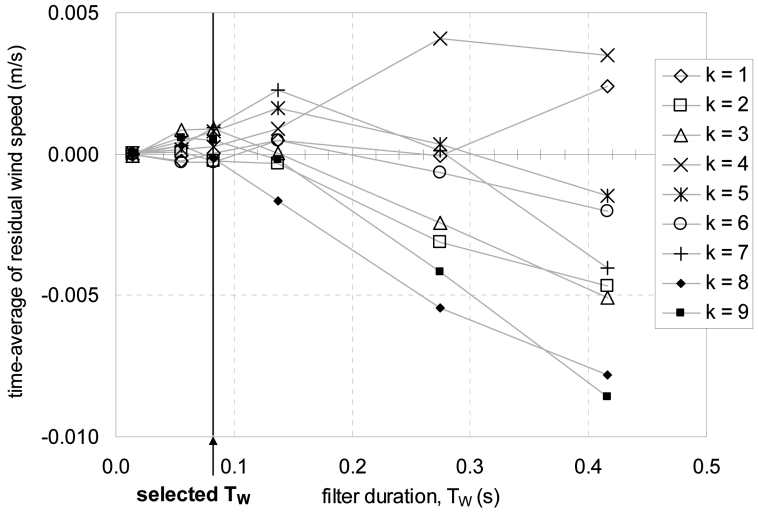

Fig. 7 Effect of moving-average filter duration on time-averaged residual wind speed (WT1 DOS, SHW probe, c = 1)

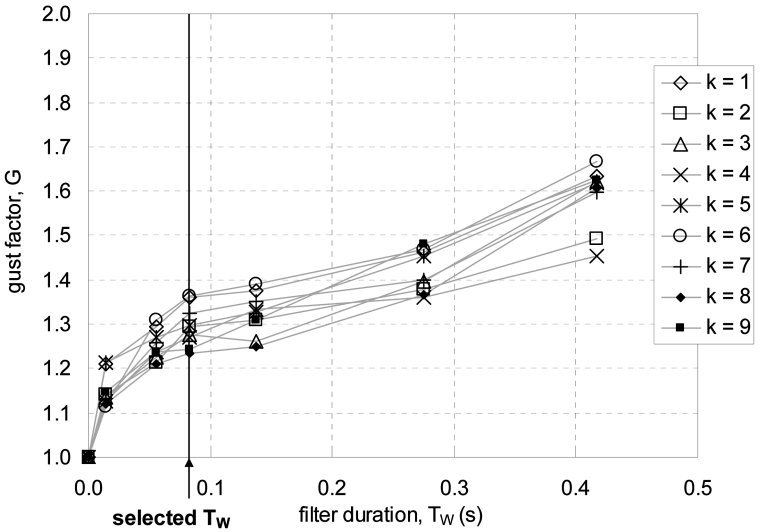

Fig. 8 Effect of moving-average filter duration on gust factor (WT1 DOS, SHW probe, c = 1)

3. Time-varying mean wind speed from simulator and field observations

Field measurements from a 2002 RFD near Lubbock, Texas, USA were conducted by Orwig and Schroeder (2007). Wind velocity was sampled at 1 Hz from a north-south line of seven towers. The spacing between adjacent towers was 263 m.

The largest observed wind speeds were $u_p \approx 40$ m/s at anemometers on Towers 1 to 4. For the outflow simulator, the peak wind speed and the two prominent changes of wind direction were of primary interest. The time segment ($t_1 \le t \le t_2$), during which the peak wind speed occurred and

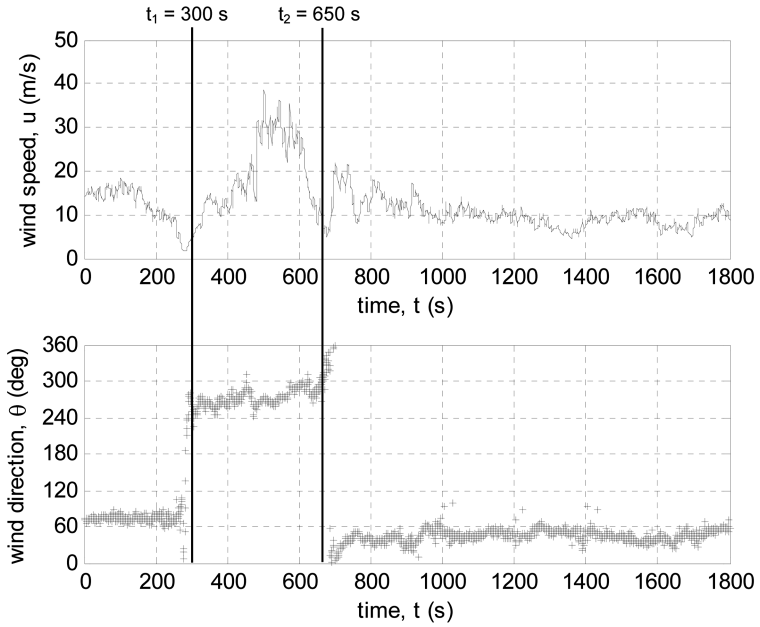

Fig. 9 Velocity history from 2002 RFD (Tower 4, 10 m AGL)

wind direction was approximately constant, was identified (Fig. 9). This portion of the wind speed record was relevant for comparison to the slot jet simulator data. The central tower in the line encountered the outflow ~ 50 seconds before the flanking towers did, which was consistent with a curved radar echo in plan view.

The 2002 RFD wind speed records were decomposed into running mean and residual components. A central moving-average scheme was used, with $T_W = 40$ s as recommended by H2008. This allowed an assessment of the WT1 DOS data against the field observations.

3.1 Comparison metrics

From a downdraft outflow wind speed record, a half-speed ($U_{0.5}$) can be determined from the peak and advective speeds, as shown by Eq. (3).

$$U_{0.5} = \frac{(U_p - U_c)}{2} + U_c \tag{3}$$

The notation in Eq. (3) is for a running mean, but the same approach applies to an ensemble-average, <U>. With an idealised wind speed signal, $U_{0.5}$ occurs exactly twice. The half-duration ($T_{0.5}$) is the duration between these two occurrences.

The dominant vortex in the outflow simulator was conveyed by the slot jet stream. At x/b = 10, a constant advective wind speed was estimated as $U_c = 2.5$ m/s. The centre of the dominant vortex was identified as shown in Fig. 3. U_c was estimated from the displacement (in pixels) of the vortex centre from one frame to the next. The results from two outflow trials indicated that the centre had approximately constant streamwise speed, at the location of interest (Fig. 10). The origin of Fig. 10 corresponds to the first video frame in which the extent of the vortex can be estimated. For

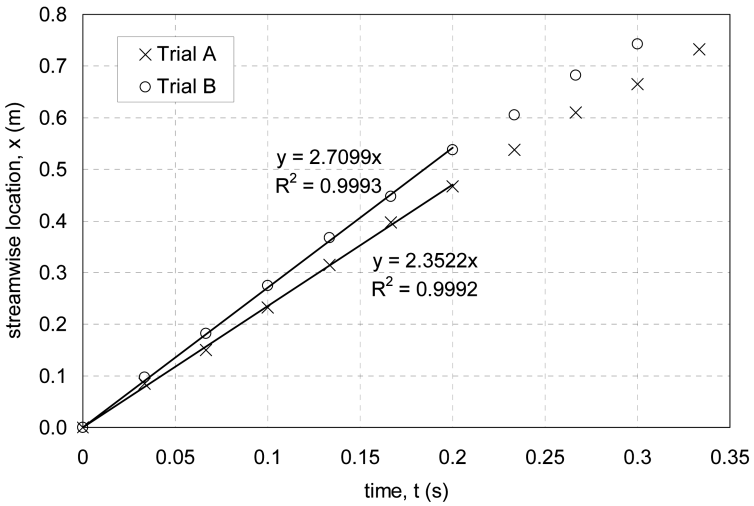

Fig. 10 Streamwise advection of the dominant vortex centre (WT1 DOS)

instance, $t = x = 0$ for the Trial A data series corresponds to Fig. 3(a). For the 2002 RFD, H2008 determined $U_c = 12$ m/s based on radar echo motion, and wind speed observations at Reese and Lubbock Airports.

U_p and $T_{0.5}$ characterised a downdraft outflow wind speed record from a fixed near-surface point. The parameters in Table 3 were determined from the WT1 DOS ensemble-averages (§2.5.1), as annotated on Fig. 5. The parameters in Table 4 were determined from the WT1 DOS running means (§2.5.2), as annotated on Fig. 6(a). The parameters in Table 5 were determined from the Lubbock downdraft outflow running means.

Simulator and full-scale wind speed histories were compared in non-dimensional form by normalising by these characteristic parameters. Peak wind speed in the simulator and full-scale records were aligned at $t/T_{0.5} = 0$. The evolution and duration, of the extreme wind speeds in full-scale versus in the simulator, were then assessed.

A simple approach for comparing the evolution was to examine the slope of piecewise linear segments of the normalised wind speed histories. The rate of change (m) of normalised wind speed with normalised time was calculated with Eq. (4).

$$m = \frac{\Delta U}{U_p} \cdot \frac{T_{0.5}}{\Delta t} \tag{4}$$

Positive slope prior to the peak wind speed and negative slope after the peak wind speed were denoted as m_1 and m_2, respectively. Additional nomenclature was required to allow for wind speed records with more than one distinct positive and one distinct negative slope. The first positive-slope segment was denoted as m_{1a}, the following one was m_{1b}, etc. The first negative-slope segment after the peak wind speed was denoted as m_{2a}, the following one was m_{2b}, etc.

The duration of the extreme wind speeds was quantified by determining the difference in time between the instant of the first up-crossing and the instant of the last down-crossing of a threshold value. Thresholds of $U/U_p = 0.6$ and 0.8 were suitable for the records examined in this study. $T_{n,\,0.6}$

Table 3 Characteristic parameters for ensemble-averaged wind speed histories (WT1 DOS)

c	K	probe	$<U>_p$ (m/s)	$<U>_{0.5}$ (m/s)	$T_{0.5}$ (s)
1	9	SHW	11.5	7.0	0.33
		CHW	10.0	6.3	0.27
2	7	SHW	12.2	7.4	0.30
		CHW	10.8	6.7	0.24
3	9	SHW	9.9	6.2	0.17
		CHW	7.5	5.0	0.20
4	10	SHW	9.8	6.1	0.14
		CHW	7.4	4.9	0.12
5	10	SHW	9.4	6.0	0.15
		CHW	7.1	4.8	0.21
6	10	SHW	9.0	5.8	0.17
		CHW	8.0	5.3	0.14
7	10	SHW	6.0	4.3	0.34
		CHW	4.9	3.7	0.22

Table 4 Characteristic parameters for running mean wind speed histories (WT1 DOS, c = 1)

c	probe	k	U_p(m/s)	$U_{0.5}$(m/s)	$T_{0.5}$(s)
1	SHW	1	11.0	6.7	0.38
		2	10.3	6.4	0.39
		3	10.9	6.7	0.30
		4	10.3	6.4	0.42
		5	10.8	6.7	0.38
		6	10.9	6.7	0.34
		7	10.5	6.5	0.36
		8	11.7	7.1	0.30
		9	10.9	6.7	0.32
		mean (K = 9)	10.8	6.7	0.35
		range/mean	13%	10%	36%
	CHW	mean (K = 9)	9.7	6.1	0.31
		range/mean	5%	4%	29%
2	SHW	mean (K = 7)	11.2	6.9	0.33
		range/mean	6%	5%	17%
	CHW	mean (K = 7)	10.0	6.3	0.30
		range/mean	15%	12%	34%

Table 5 Characteristic parameters for running mean wind speed histories (2002 RFD)

Tower	Anemometer height (m AGL)	U_p (m/s)	$U_{0.5}$ (m/s)	$T_{0.5}$ (s)
1	3	28.5	20.3	83
3	10	31.5	21.8	154
4	2	29.5	20.8	144
4	4	31.1	21.6	143
4	6	29.8	20.9	140
4	10	31.1	21.5	139
4	15	31.8	21.9	140
5	3	29.1	20.5	139
5	6	29.2	20.6	136
5	10	30.1	21.1	137
6	10	27.7	19.9	158
7	3	25.4	18.7	149
	mean	29.6	20.8	138.5

and $T_{n,\,0.8}$ corresponded to the former and latter threshold values, respectively. These two durations and the slopes of the piecewise linear segments of the wind speed histories were the characteristic parameters of interest for comparing full- and model-scale normalised wind speed histories (Table 6).

A comparison of the simulator flow to the Lubbock outflow characterised the facility performance and identified possible refinements of the simulator test conditions. With Fig. 11, the ensemble-averaged wind speed record at the simulator mid-span (c = 1) was compared to the 2002 RFD Tower 4 records. A decrease of m_1 magnitude and an increase of m_{2b} magnitude in the simulator would have more closely emulated the Tower 4 observations. The simulator $T_{n,\,0.6}$ and m_2 values matched the Tower 4 values well.

The normalised wind speed histories at 10 m AGL from Towers 4, 5 and 6 were very similar. The three towers spanned a full-scale horizontal distance of 526 m. Tower 4 and simulator data were compared (Fig. 12). The simulator wind speed histories were all for the same height (y/b = 0.63). The spacing of the three measurement locations covered 80% of the tunnel span as shown, with the Lubbock anemometer layout at 1:1200 length scaling, in Fig. 13. Bearing in mind that the small-

Table 6 Comparison of normalised wind speed history characteristics

Case	Slope		Duration	
	m_1	m_2	$T_{n,\,0.6}$	$T_{n,\,0.8}$
2002 RFD, Tower 4, 15 m AGL	1.6	-0.3 -1.6	1.10	0.84
2002 RFD, Tower 5, 10 m AGL	3.0 0.8	-0.1 -1.5	1.08	0.89
WT1 DOS, c = 1, SHW	2.0	-0.3 -1.5	1.11	0.71

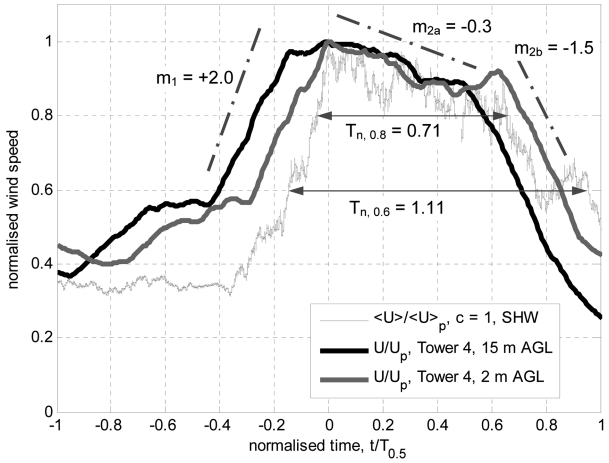

Fig. 11 Comparison of wind speed histories from WT1 DOS (c = 1, SHW) and 2002 RFD (Tower 4)

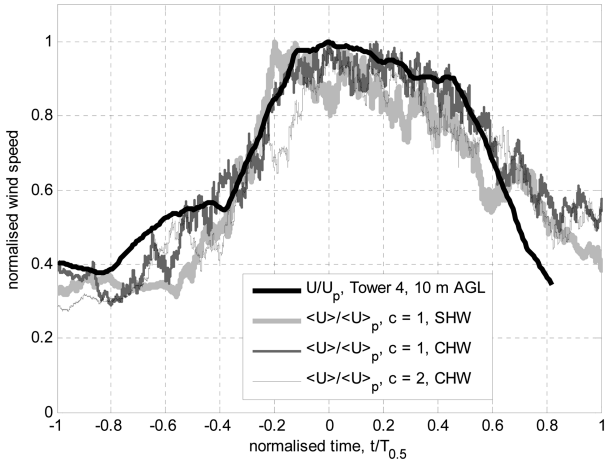

Fig. 12 Variation of wind speed history with span-wise location (WT1 DOS) compared to 2002 RFD (Tower 4, 10 m AGL)

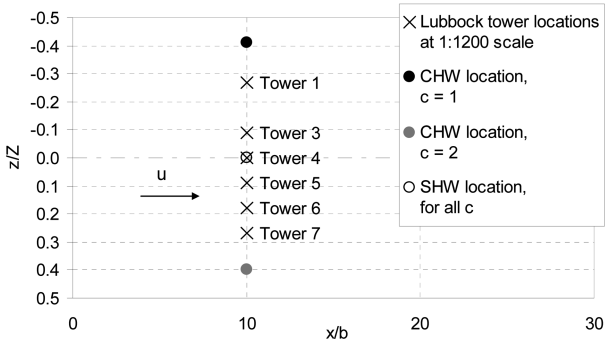

Fig. 13 Comparison of probe locations for the WT1 DOS and 2002 RFD data sets

scale fluctuations of the ensemble-averaged wind speed histories would be smoothed with increased ensemble size, the simulator outflow exhibited a similar degree of span-wise uniformity as the full-scale outflow, over a much larger scaled span.

3.2 Length scaling of the coarse flow features

For modelling purposes, the ratio of the spatial size of the simulator outflow to that of the Lubbock outflow was of interest. A ratio of characteristic times and a ratio of characteristic velocities were determined from Eqs. (5) and (6), respectively. Length scale, based on the horizontal extent of intense winds, was estimated from Eq. (7). The simulator numerical values were shown in Table 4 (c = 1, SHW, mean, K = 9). The full-scale numerical values were shown in Table 5 (Tower 4, 15 m AGL).

$$\lambda_T = \frac{(T_{0.5})_{\text{model-scale}}}{(T_{0.5})_{\text{full-scale}}} = \frac{0.35\text{s}}{140\text{s}} = \frac{1}{400} \tag{5}$$

$$\lambda_v = \frac{(U_p)_{\text{model-scale}}}{(U_p)_{\text{full-scale}}} = \frac{10.8\ \text{m/s}}{31.8\ \text{m/s}} = \frac{1}{2.94} \tag{6}$$

$$\lambda_L = \frac{\ell_{\text{model-scale}}}{\ell_{\text{full-scale}}} = \frac{(T_{0.5})_{\text{model-scale}} \cdot (U_p)_{\text{model-scale}}}{(T_{0.5})_{\text{full-scale}} \cdot (U_p)_{\text{full-scale}}} = \lambda_T \cdot \lambda_v \approx \frac{1}{1200} \tag{7}$$

A 1:1200 length scaling is small for structural modelling, but the following two points are important. First, a rear-flank downdraft is on the larger end of the range of observed downdraft size. Microburst events, with comparable or greater wind speeds, likely occur at a physical size approaching an order of magnitude smaller than the 2002 RFD (i.e., $\lambda_L \sim 1{:}120$). These smaller outflows may indeed turn out to be the design case for most structures. Second, the simulator conditions can be varied. Increased blower speed will increase $(U_p)_{\text{model-scale}}$ and λ_L. Furthermore, $(U_p)_{\text{model-scale}}$ and λ_L may be increased by modifying the gate actuation.

4. Residual wind speed from simulator and field observations

Classical time series analysis rests on the assumption that the signal to be analysed is at least weakly statistically stationary. Residual wind speed records were examined in the following section and the stationarity assumption was evaluated. The distribution, relation to the mean wind speed, auto-correlation, and auto-spectrum of the residual wind speed component were examined.

4.1 Stationarity

A time series is weakly stationary if the window of samples, from which the mean and mean square (MS) values were calculated, can be shifted in time without affecting these two values (Bendat and Piersol 1986). Priestley (1988, Section 1.2) noted that this assumption is a mathematical idealisation and in practice, "the most one could hope for is that ... the series would not depart 'too far' from stationarity for the results of the analysis to be invalid." The stationarity of the residual wind speed histories was examined about the time of occurrence of U_p. The moving-average

procedure yielded a residual component with a near-zero time-average. The time-averaged residual component (H2008, Fig. 6) was not expected to vary significantly with time-shifting, since the averaging window duration was long relative to the short-period fluctuations of the residual wind speed. The MS residual wind speed was given further attention.

First, the effect of averaging window duration on MS residual was examined with a window centred at the sample corresponding to U_p occurrence. In Fig. 14, for example if $T_W = 201$, the window of samples (from which MS residual was determined) had 100 samples before and after the sample corresponding to U_p occurrence. By increasing the number of samples on both ends of the window, the variation of MS residual was calculated. The Fig. 14 results were due to the residual wind speed characteristics and the imposed window symmetry. The largest fluctuations occurred about the window centre that coincides in time with U_p, so MS residual attained its largest value at small T_W. As T_W increased, more small fluctuation samples were included in the averaging procedure. Eventually, the small fluctuation samples formed most of the window, resulting in a stable MS residual at large T_W. However, the most appropriate averaging time would be an intermediate value that had neither the large variability at small values nor the inclusion of many small fluctuations that were unrepresentative of the extreme winds. The half-duration from §3.1 was readily identified in typical outflow wind speed histories and served as appropriate averaging window duration. The MS residual, as calculated over the half-duration, was identified on Fig. 14. In general, $T_{0.5}$ was not exactly symmetric about the occurrence of U_p, so there was a slight deviation from the line calculated from a symmetric window. Calculated from the half-duration, MS residual showed a consistent increasing trend as the probe height decreased.

With averaging window duration equal to the half-duration, the stationarity of the MS residual wind speed was examined. For a stationary signal, the MS residual should be independent of the averaging window location in the time series. As the averaging window was shifted in time over the residual-squared time series, the MS residual varied as shown by Fig. 15. The window location (indicated on the abscissa) was in terms of the location of the centre sample of the window. The abscissa datum corresponded to the occurrence of U_p. The range of the plotted points corresponded to shifting the window centre over the half-duration. Locally stationary residual wind speed segments were identified (Fig. 15 arrows). Examining all available records near peak gust, residual wind speed exhibited local stationarity at the central towers in the line (Towers 4, 5, 6), but not at the peripheral towers (1, 3, 7). Near the instant of peak gust occurrence at Tower 4, local

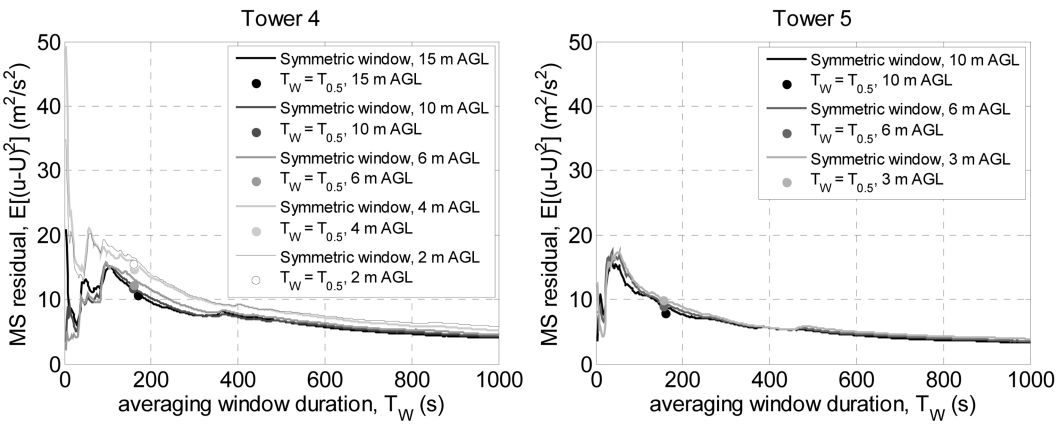

Fig. 14 Dependency of mean square residual wind speed on averaging window duration (2002 RFD)

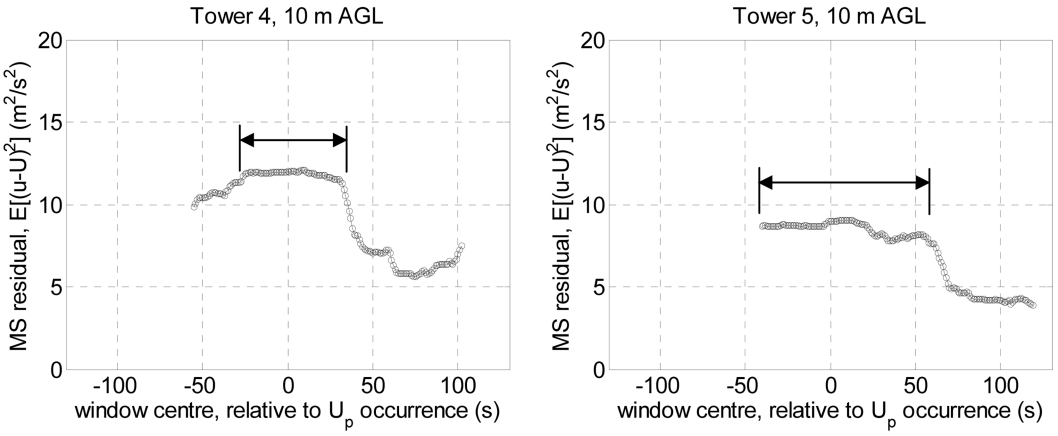

Fig. 15 Dependency of mean square residual wind speed on averaging window location (2002 RFD; results shown for averaging window location moved over the half-duration)

stationarity improved with increasing height AGL. The simulated outflow was analysed in the same manner and the findings from Fig. 16 were similar to the preceding results for the 2002 RFD.

4.2 Residual wind speed distribution

§ 4.1 showed some observed and simulated residual wind speed histories that are weakly stationary, locally about the occurrence of the peak running mean wind speed. As explained by Priestley (1988, Section 1.3), a weakly stationary random process is completely stationary, provided it is also a Gaussian (i.e., normal) process. Probability density distributions from Lin (2010) confirmed that some downdraft outflow residual wind speed history segments, which were locally stationary and near the instant of peak gust occurrence, conformed to an equivalent normal distribution. In particular, histograms for central locations in the tower line at, or above, 10 m AGL were reasonably symmetric, conformed well to their equivalent normal distribution, and did not show distortions that may arise from lack of stationarity (e.g., large excess kurtosis or multiple modes).

4.3 Residual wind speed relative to mean wind speed

Peak gust and peak running mean wind speeds were determined for all simulation trials and configurations. The portion of the peak wind speed values in the WT1 DOS attributable to the residual component was determined (Fig. 17). The largest peak wind speeds occurred at the configurations where the probe was closest to the tunnel floor. For c = 1 and 2, $\langle u_p \rangle$ exceeded $\langle U_p \rangle$ by approximately 30% of the latter. As expected for measurement locations below the axis of the dominant vortex, peak wind speed diminished with increasing height.

A gust factor indicated the magnitude of the residual component relative to the mean component. Gust factor was found from a ratio of the peak wind speed to the peak running mean wind speed, as shown by Eq. (8). By using peak values, this definition related two quantities of primary interest, and was a simple and convenient metric.

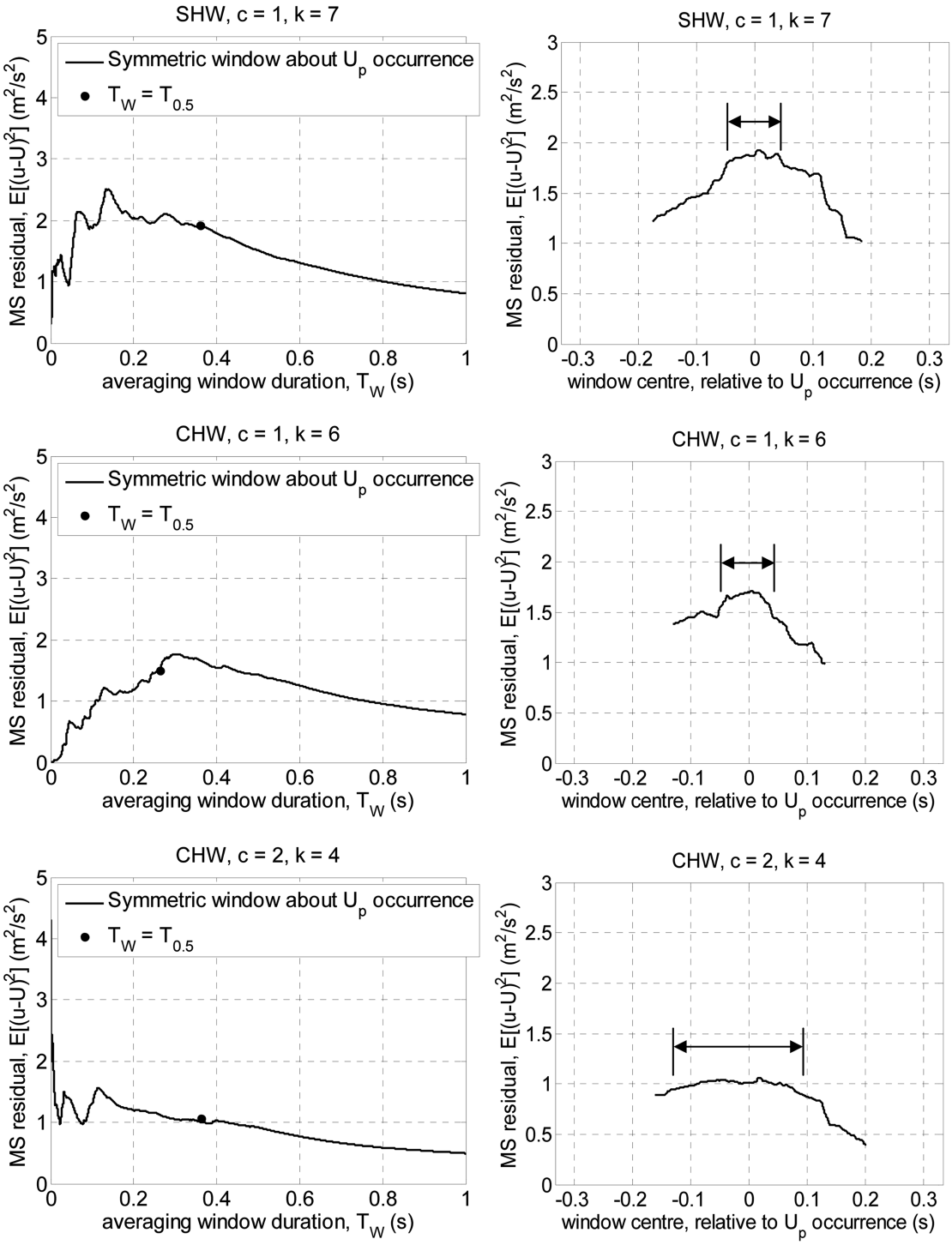

Fig. 16 Dependency of mean square residual wind speed on averaging window duration and location (WT1 DOS)

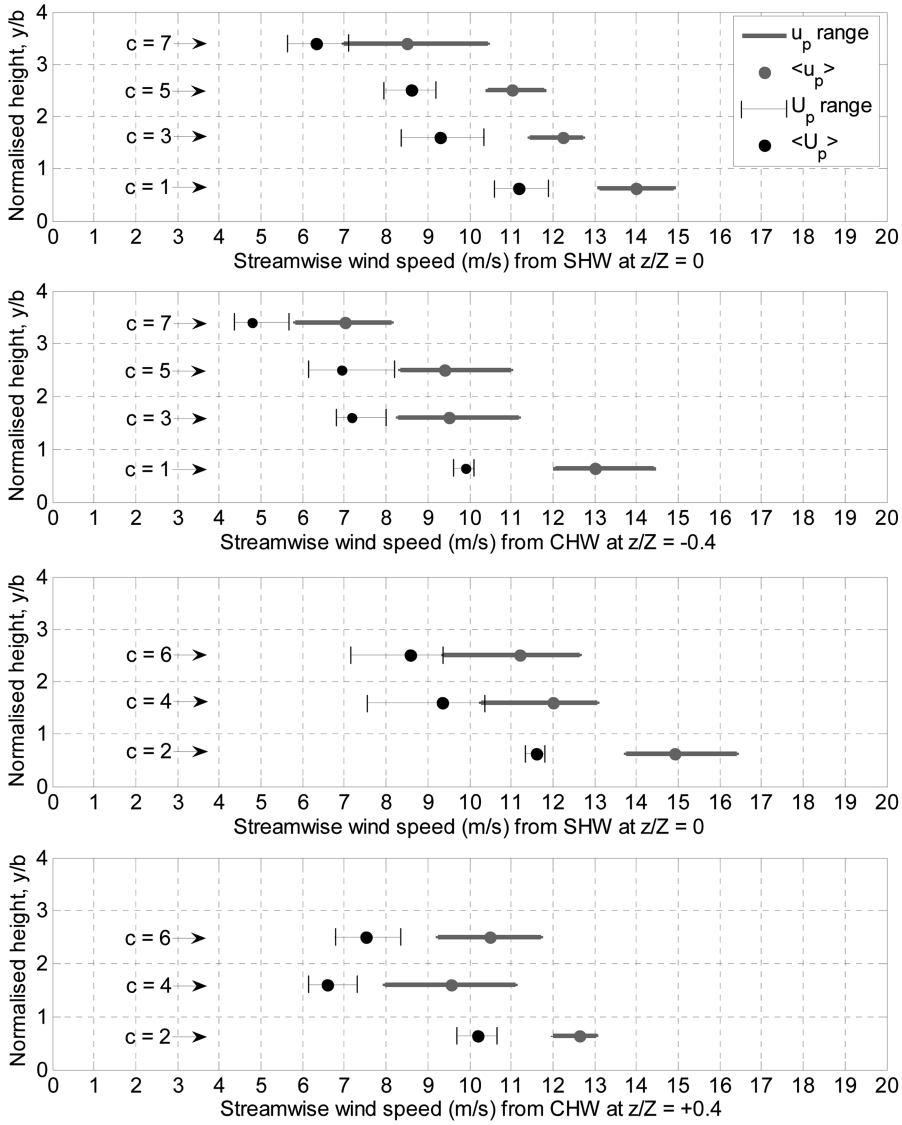

N.B. A dot represents the ensemble-average for each configuration. The attached bars indicate the range of peak values in that ensemble.

Fig. 17 Vertical profiles of peak wind speed (WT1 DOS)

$$G = \frac{u_p}{U_p} \tag{8}$$

For c = 1 and 2 in Fig. 18, <G> generally varied between 1.25 and 1.45. For the 2002 RFD, H2008 reported $G \approx 1.25$ for a height range of 2 to 15 m AGL. Ensemble-averaged gust factor and gust factor variability appeared to be directly related to height above ground. <G> approached a maximum value of 1.5. The range of G over an ensemble tended to increase fairly consistently with increasing height.

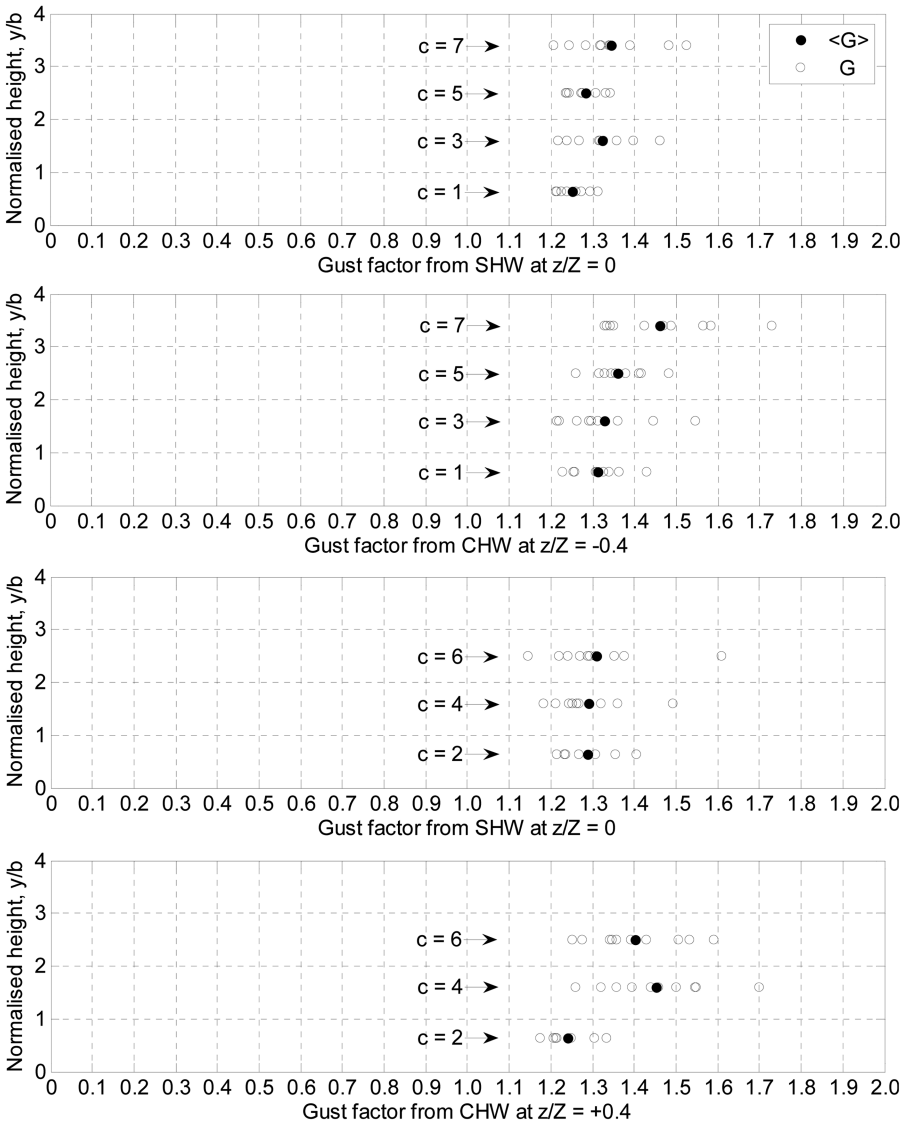

N.B. An unfilled circle represents gust factor for an individual trial. A filled circle represents gust factor for the ensemble mean.

Fig. 18 Vertical profiles of gust factor (WT1 DOS)

H2008 extended the traditional definition of turbulence intensity (for a statistically stationary record) to examine non-stationary wind speed. Eq. (9) defines time-varying turbulence intensity. The overbar denotes a moving-average with T_W from § 2.5.2.

$$I_u(t) = \frac{\sqrt{\overline{(u(t)-U(t))^2}}}{U(t)} = \frac{(u(t)-U(t))_{RMS}}{U(t)} \tag{9}$$

This definition of turbulence intensity is an instantaneous ratio of time-varying standard deviation and mean. Standard deviation is a simple measure of fluctuation magnitude, but it provides no information about whether deviations are exceedances or deficits from the mean. Where the number of exceedances and deficits from the mean are significantly unequal, standard deviation does not provide a fully adequate description of the process. Thus, Eq. (9) is relevant for residual wind speed histories that are symmetrically-distributed, as discussed in § 4.2. Furthermore, large I_u results from the following two possibilities: (1) large $(u\text{-}U)_{RMS}$ with moderate U, or (2) small U with moderate $(u\text{-}U)_{RMS}$. At the least, some commentary on the relative importance of the numerator and denominator, at instants of interest, helps clarify this ambiguity.

The 2002 RFD had peak I_u in excess of 30% (Fig. 19). By examining the time variations of the three signals in Fig. 19, it was apparent where peak I_u resulted from either a RMS residual peak or a U trough. Moreover, I_u did not peak - it remained moderate at 10 to 15% - when U_p occurred. For the WT1 DOS, peak I_u was between 20 and 30% as indicated by Fig. 20. When U_p occurred, I_u was between 8 to 15%.

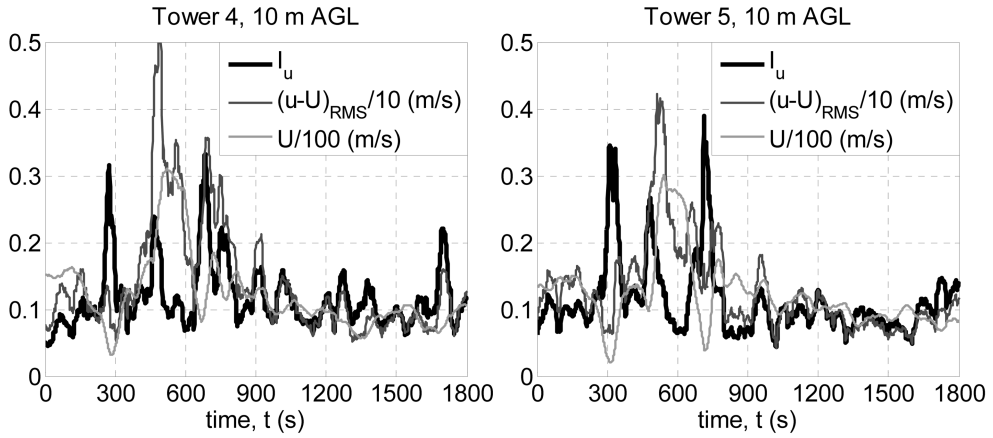

Fig. 19 Turbulence intensity, RMS residual and moving-averaged wind speed histories (2002 RFD)

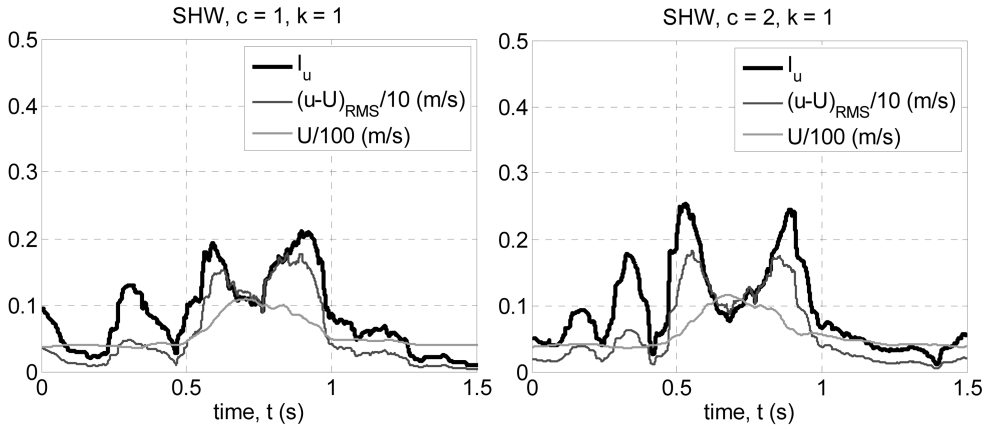

Fig. 20 Turbulence intensity, RMS residual and moving-averaged wind speed histories (WT1 DOS)

4.4 Correlation and spectral analysis

The examined residual wind speed segments were the locally stationary durations near the occurrence of U_p, as identified in § 4.1. The auto-correlation coefficient function was computed with Eq. (10) and plotted in Fig. 21. The integral time scale was computed from Eq. (11).

$$\rho_{ss} = \rho_{ss}(\tau) = \frac{E[(s(t) - \bar{s}) \cdot (s(t+\tau) - \bar{s})]}{\overline{s^2}}, \text{ where } s = u\text{-}U \tag{10}$$

$$T_I = \int_0^{\text{first abscissa crossing}} \rho_{ss}(\tau) \cdot d\tau \tag{11}$$

Between the limits of $\tau = 0$ and the first abscissa crossing, the integral was evaluated by trapezoidal numerical integration. T_I was a consistent value during peak wind intensity at Towers 4 and 5, and ~ 30% longer at Tower 6, as summarised by Table 7. An identical analysis was performed with the WT1 DOS data and integral time scales were determined (Fig. 22 and Table 8).

The power spectral density of residual wind speed was determined by spectral estimation (Welch 1967). Each 2002 RFD residual wind speed record was divided into segments of thirty-two samples that overlapped by 25% of segment size. WT1 DOS residual wind speed records were broken into

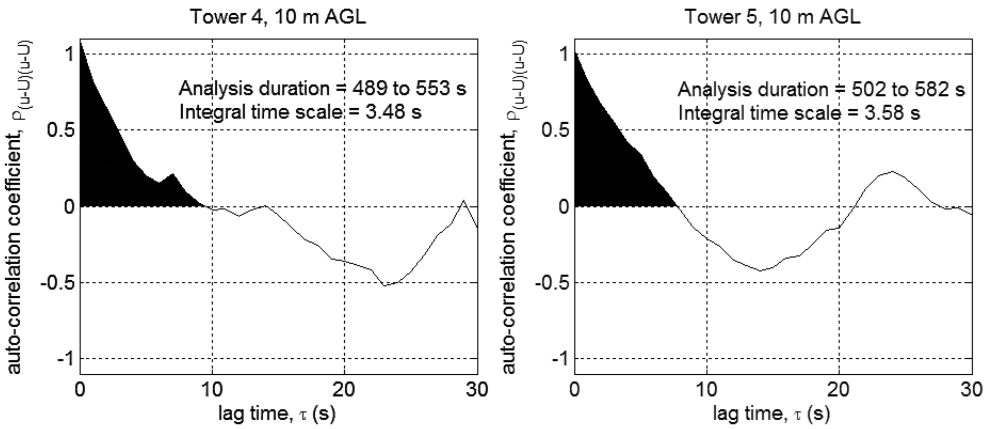

Fig. 21 Integral time scale of residual wind speed fluctuations (2002 RFD; locally stationary and near-U_p duration only)

Table 7 Integral time scale of residual wind speed (2002 RFD)

Tower	Anemometer height (m AGL)	T_I (s)
4	6	3.24
4	10	3.48
4	15	3.25
5	6	3.37
5	10	3.58
6	10	4.50
	mean	3.6

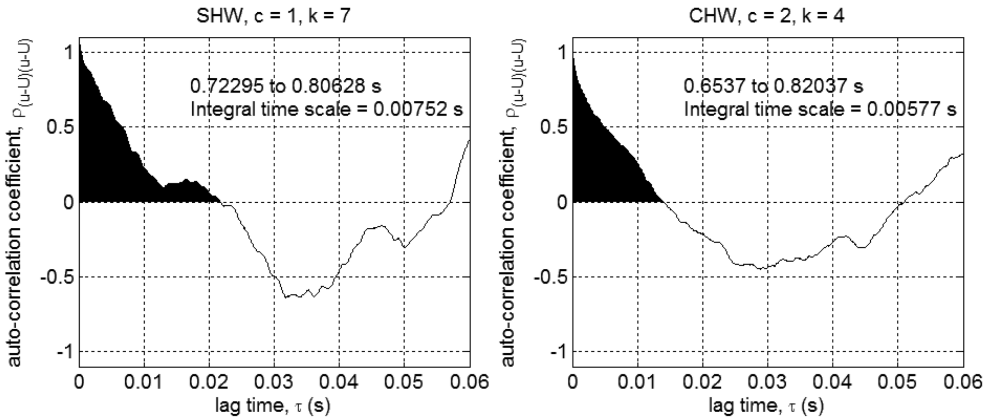

Fig. 22 Integral time scale of residual wind speed fluctuations (WT1 DOS; locally stationary and near-U_p duration only)

Table 8 Integral time scale of residual wind speed (WT1 DOS)

c	probe	k	T_I (s)
1	SHW	7	0.00752
1	CHW	6	0.00189
2	CHW	4	0.00577
		mean	0.005

overlapping segments of two-hundred fifty-six samples. A Hamming window (to reduce the spectral bias that may arise from abruptly truncating the complete record into segments) and then a Fast Fourier Transform were applied to each segment. The periodogram of each segment was calculated and averaged to obtain the spectrum estimate. By scaling the spectrum estimate by the wind speed sampling frequency, $S_{(u-U)(u-U)}$ was computed (i.e., power per unit frequency). The auto-spectrum was normalised according to Eqs. (12) and (13), and the field and simulator data were plotted together as Fig. 23.

$$\text{normalized spectral density} = \frac{f \cdot S_{(u-U)(u-U)}}{(u-U)^2} \tag{12}$$

$$\text{Strouhal number} = f \cdot T_I \tag{13}$$

The frequency resolution of the WT1 DOS measurements was much higher than that of the 2002 RFD measurements. The normalized spectra of the two data sets matched up in a well-aligned curve. Towards the large energy-containing scales of fluid motion, the slope of the residual wind speed auto-spectra for the rear-flank downdraft outflow was approximately -5/3. The dissipative spectral range was characterised by a -14/3 power relation.

4.5 Length scaling of the fine flow features

The full-scale and simulator integral time scales near the peak gust were approximately four

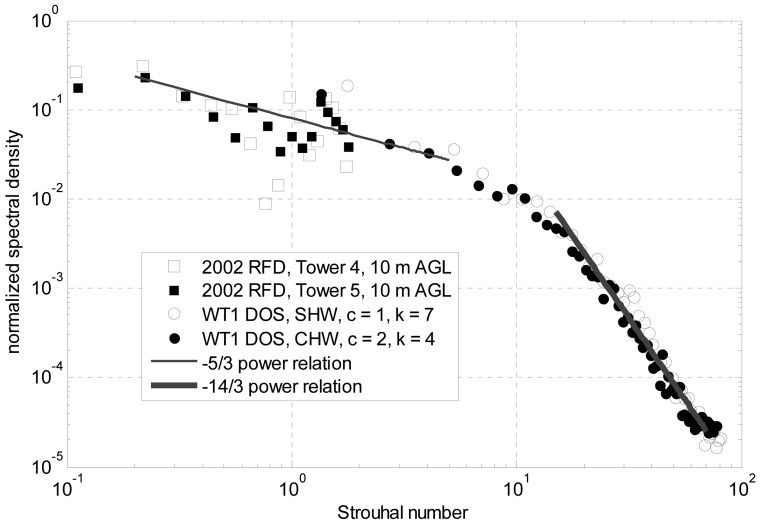

Fig. 23 Auto-spectral density of residual wind speed fluctuations

seconds and on the order of milliseconds, respectively. A ratio of characteristic times and a ratio of characteristic velocities were determined with Eqs. (14) and (15), respectively. Length scale was estimated with Eq. (16).

$$\lambda_T = \frac{(T_I)_{model-scale}}{(T_I)_{full-scale}} = \frac{0.00752s}{3.25s} = \frac{1}{432} \tag{14}$$

$$\lambda_v = \frac{(U_p)_{model-scale}}{(U_p)_{full-scale}} = \frac{10.8\ m/s}{31.8\ m/s} = \frac{1}{2.94} \tag{15}$$

$$\lambda_L = \frac{\ell_{model-scale}}{\ell_{full-scale}} = \frac{(T_I)_{model-scale} \cdot (U_p)_{model-scale}}{(T_I)_{full-scale} \cdot (U_p)_{full-scale}} = \lambda_T \cdot \lambda_v \approx \frac{1}{1300} \tag{16}$$

Full-scale and simulator characteristic times were from Table 7 (Tower 4, 15 m AGL) and Table 8 (c = 1, SHW, k =7), respectively. Full-scale and simulator characteristic velocities were from Table 5 (Tower 4, 15 m AGL) and Table 4 (c = 1, SHW, mean, K = 9), respectively. The fine flow structure in the simulator was estimated as being 1300 times smaller in spatial size than the 2002 RFD fine flow structure.

5. Conclusions

The performance of the WT1 DOS was thoroughly validated against field observations. At the slot nozzle exit, across most of the slot height, the mean wind speed profile exhibited uniformity within ± 4% of the bulk wind speed. The corresponding turbulence intensity profiles lay within 2 to 6%. The wake of the slot top plate was negligible. The displacement and momentum thicknesses of the boundary layer at the bottom face of the plate were 2%, or less, of the slot height. Nozzle

conditions can be refined by installing honeycomb in the slot. Given the engineering challenges of this large facility, the initial jet conditions were good.

The test section for transient downdraft outflow experiments extended to approximately 20 slot heights downstream of the nozzle. The flow visualisation confirmed that the facility generated a dominant vortex that grew with distance from the slot. The trial-to-trial repeatability of the simulator was as good as expected for a turbulent flow simulation. All wind speed records showed the expected characteristics of a downburst outflow, and running mean wind speed histories were generally within ± 10% of their ensemble-average. Increasing the ensemble size by an order of magnitude would remove the high-frequency components of the ensemble-average and allow a more accurate assessment of the ergodicity of the simulated outflow.

A moving-average procedure worked well with the simulated outflow wind speed records. The H2008 selection criteria for moving-average filter duration yielded similar dimensionless filter durations for the 2002 RFD and the WT1 DOS data. Appropriate filter duration appeared to be 25% of the half-duration ($T_{0.5}$). Beyond these specific findings, a framework for normalising and comparing full-scale and simulated wind speed histories was presented. Peak wind speed and half-duration indicated the intensity and horizontal extent of the damaging winds, respectively. The success in simulating a target signal was assessed with the slope of piecewise linear segments of the wind speed history and the duration over which wind speed exceeds a threshold.

With analysed records that exhibited statistical stationarity, the methods of classical time series analysis produced a valid quantitative description of downdraft outflow residual wind speed. Near the instant of peak gust occurrence, some 2002 RFD and WT1 DOS residual wind speed histories exhibited weak stationarity and a normal distribution, which was suggestive of complete statistical stationarity at the peak gust. For the 2002 RFD, stationarity was most evident for the wind speed records at central locations in the line of observation towers. Residual wind speed stationarity was evident at all three spanwise locations examined for the WT1 DOS.

H2008 reported a gust factor of 1.25 for the wind speed records at 2 to 15 m AGL. Ensemble-averaged gust factor in the simulator was in the range of 1.25 to 1.3 at near-surface locations. For the full-scale peak gust, I_u was in the range of 10 to 15%. For the simulated peak gust, I_u was in the range of 8 to 15%. With respect to parameters that relate the mean and residual components, the simulated flow matched the full-scale benchmark particularly well. Near the instant of peak gust occurrence, auto-spectra of the full-scale and simulator residual wind speed were described by a power relation (between spectral density and frequency) with an exponent of -5/3 for the large scales of motion and -14/3 for the dissipative range.

Based on the half-duration of the time-varying mean wind speed, the coarse horizontal flow structure of the simulated outflow was estimated as 1200 times smaller in spatial size than the 2002 RFD. Based on the integral time scale of the residual wind speed, the simulated fine flow structure was estimated as 1300 times smaller in spatial size than the fine flow structure in the 2002 RFD. This close agreement, across the range of scales of the turbulent motion, was remarkable. Furthermore, the 8% discrepancy between the coarse and fine length scaling was within the range that can be explained by propagation of uncertainty in wind speed measurements from the simulator and field studies.

Keeping in mind the variability of impinging downdraft size, the 2002 RFD was at the large end of the range. For instance, Wakimoto (2001, Section 7.4) discussed RFDs of ~ 5000 m scale. Fujita and Wakimoto (1981, Fig. 1) indicated microburst damage patterns of < 1000 m scale, which would suggest outflow vortex size of ~ 100 m. These microburst outflows would be modelled at 1:100 to

1:500 length scaling in the WT1 DOS, i.e., a range of scaling comparable to that of conventional boundary layer wind tunnels.

A marriage of photographic evidence and wind speed measurements for a single full-scale event has proven to be elusive. When such simultaneous observations are available, it will be interesting to see how the present approach of estimating length scale (from time and velocity scales) compares to directly taking a ratio of characteristic lengths. To completely describe an outflow event would also require a vertical coarse length scale (e.g., outflow depth). When outflow depth is available with more accuracy, it would make sense to set (1) a vertical length scaling based on the ratio of the simulator slot height to the outflow depth and (2) a gate actuation duration that yields an equivalent horizontal coarse length scaling.

This article presented a viable approach to physical modelling of a high-intensity downdraft outflow. In the opinion of the authors, this is a promising approach to facilitate structural model testing. Alternatively, an impinging jet approach is clearly favourable when complete similarity of the downdraft and outflow are essential to the goals of the experiment. The cost exacted for this improvement is a much larger and more expensive facility to achieve an equivalent physical outflow scale. This additional cost is estimated as one order of magnitude in facility footprint area and two orders of magnitude in price.

Acknowledgements

The authors acknowledge Dr. J.K. Galsworthy, Dr. D. Surry, and the staff at the UWO BLWTL for their support of this work. Mr. C. Vandelaar and Dr. J.P.C. King led the design and implementation of the structural additions to BLWT1. The anemometry system used in this study was provided by Dr. G.A. Kopp and Dr. R.J. Martinuzzi. Dr. J.L Schroeder at Texas Tech University kindly made the 2002 Lubbock downdraft raw data available. Discussions with Dr. J.D. Holmes about his 2008 article were constructive.

The first author thanks the Natural Sciences and Engineering Research Council of Canada (NSERC) and the Association of Universities and Colleges of Canada for financial support through scholarships. This research was made possible through funding of facility costs by NSERC, Manitoba Hydro, the Centre for Energy Advancement through Technological Innovation and the Institute for Catastrophic Loss Reduction.

References

Bendat, J.S. and Piersol, A.G. (1986), *Random data: Analysis and measurement procedures*, 2nd Edition, John Wiley & Sons, USA.

Choi, E.C.C. and Hidayat F.A. (2002), "Dynamic response of structures to thunderstorm winds", *Prog. Struct. Eng. Mater.*, **4**(4), 408-416.

Fujita, T.T. (1981), "Tornadoes and downbursts in the context of generalized planetary scales", *J. Atmos. Sci.*, **38**(8), 1511-1534.

Fujita, T.T. and Wakimoto, R.M. (1981), "Five scales of airflow associated with a series of downbursts on 16 July 1980", *Mon. Weather Rev.*, **109**(7), 1438-1456.

Holmes, J.D., Hangan, H.M., Schroeder, J.L., Letchford, C.W., and Orwig, K.D. (2008), "A forensic study of the Lubbock-Reese downdraft of 2002", *Wind Struct.*, **11**(2), 137-152.

Letchford, C.W. and Chay, M.T. (2002), "Pressure distributions on a cube in a simulated thunderstorm downburst. Part B: moving downburst observations", *J. Wind Eng. Ind. Aerod.*, **90**(7), 733-753.
Letchford, C.W., Mans, C. and Chay, M.T. (2002), "Thunderstorms – their importance in wind engineering (a case for the next generation wind tunnel)", *J. Wind Eng. Ind. Aerod.*, **90**(12-15), 1415-1433.
Lin, W.E. and Savory, E. (2006), "Large-scale quasi-steady modelling of a downburst outflow using a slot jet", *Wind Struct.*, **9**(6), 419-440.
Lin, W.E., Orf, L.G., Savory, E. and Novacco, C. (2007), "Proposed large-scale modelling of the transient features of a downburst outflow", *Wind Struct.*, **10**(4), 315-346.
Lin, W.E. (2010), *Validation of a novel downdraft outflow simulator: A slot jet wind tunnel*, PhD thesis, The University of Western Ontario, Canada.
Mason, M.S., Letchford, C.W. and James, D.L. (2005), "Pulsed wall jet simulation of a stationary thunderstorm downburst, Part A: Physical structure and flow field characterization", *J. Wind Eng. Ind. Aerod.*, **93**(7), 557-580.
McConville, A.C., Sterling, M. and Baker, C.J. (2009), "The physical simulation of thunderstorm downbursts using an impinging jet", *Wind Struct.*, **12**(2), 133-149.
Orwig, K.D. and Schroeder, J.L. (2007), "Near-surface wind characteristics of extreme thunderstorm outflows", *J. Wind Eng. Ind. Aerod.*, **95**(7), 565-584.
Priestley, M.B. (1988), *Non-linear and non-stationary time series analysis*, Academic Press, London, UK.
Sengupta, A. and Sarkar, P.P. (2008), "Experimental measurement and numerical simulation of an impinging jet with application to thunderstorm microburst winds", *J. Wind Eng. Ind. Aerod.*, **96**(3), 345-365.
Wakimoto, R.M. (2001), "Convectively driven high wind events", *Meteorol. Monogr.*, **28**(50), 255-298.
Walker, G.R. (1992), "Wind engineering beyond the boundary layer wind tunnel", *J. Wind Eng. Ind. Aerod.*, **41**(1-3), 93-104.
Welch, P.D. (1967), "The use of Fast Fourier Transform for the estimation of power spectra: A method based on time averaging over short, modified periodograms", *IEEE Trans. Audio Electroacoust.,* **15**(2), 70-73.
White, F.M. (2003), *Fluid mechanics*, 5th Edition, McGraw Hill, USA.

JH

Nomenclature

b	slot nozzle height
c	hot-wire probe configuration index
E[•]	expected value operator
f	frequency
f_s	sampling frequency
G	gust factor
H	shape factor = δ^*/Θ
I_u, I_v	turbulence intensity
k	ensemble index
K	ensemble size = total no. of simulator trials for a fixed set of conditions
ℓ	characteristic length
m	slope of a piecewise linear segment of a wind speed history; see Eq. (4)
maximum	largest value over space
M	filter size (no. of samples)
N	total no. of samples (forming a single record)
peak	largest value over time (at a fixed point)
$\bullet_p$	peak value operator

R^2	squared correlation coefficient (regression)
S_{ss}	auto-spectral density estimate for an input signal s
t	time
T_I	Eulerian integral time scale (i.e., de-correlation time of turbulence)
T_W	averaging window duration
$T_{n,\alpha}$	duration between a pre- and a post-peak occurrence of $U/U_p = \alpha$
$T_{0.5}$	half-duration = duration between a pre- and a post-peak occurrence of $U_{0.5}$
u	wind speed (as acquired from anemometer)
U	moving-averaged wind speed (i.e., running mean)
U_c	advective wind speed
$U_{0.5}$	half-speed for a U record; see Eq. (3)
x	distance downstream of the slot exit
X	wind tunnel length
y	distance above the working section floor
Y	wind tunnel working section height
z	distance from the wind tunnel centreline
Z	wind tunnel span
α	threshold U/U_p value for determining a characteristic duration
δ^*	displacement thickness
$\Delta\bullet$	finite change of a variable
λ_L	ratio of characteristic lengths
λ_T	ratio of characteristic times
λ_V	ratio of characteristic velocities
Θ	momentum thickness
ρ_{ss}	auto-correlation coefficient for an input signal s
τ	auto-correlation lag duration
$\{\bullet\}$	random process
$\langle\bullet\rangle$	ensemble-average operator
$\overline{\bullet}$	time-average operator

Abbreviations

AGL	above ground level
CHW	cross hot-wire
H2008	Holmes *et al.* (2008)
MS	mean square
RMS	root mean square
SHW	single hot-wire
UWO	University of Western Ontario
WT1 DOS	Wind Tunnel 1 downdraft outflow simulator
2002 RFD	rear-flank downdraft outflow near Lubbock in 2002